Arabian Journal of Chemistry (2020) 13, 6966–6976

King Saud University

Arabian Journal of Chemistry

www.ksu.edu.sa
www.sciencedirect.com

REVIEW ARTICLE

Studies on anticancerious and photocatalytic activity of carboxymethyl cellulose-cl-poly(lactic acid-co-itaconic acid)/ZnO-Ag nanocomposite

Deepak Pathania [a,*], Swadeep Sood [b], Adesh K. Saini [c], Sarita Kumari [d], Shilpi Agarwal [d], Vinod Kumar Gupta [e,*]

[a] *Department of Environmental Science, Central University of Jammu, Bagla (Rahya-Suchani), Samba, Jammu & Kashmir 181143, India*
[b] *Department of Chemistry, Government College, Dhaliara Kangra, Himachal Pradesh 177103, India*
[c] *Department of Biotechnology, MMEC, Maharishi Markandeshwar (Deemed to be University), Mullana, Ambala, Haryana, 133207, India*
[d] *Department of Zoology, Saifia Science College, Bhopal, Madhya Pradesh, India*
[e] *Department of Biological Sciences, Faculty of Science, King Abdulaziz University, Jeddah, Saudi Arabia*

Received 14 April 2020; accepted 1 July 2020
Available online 9 July 2020

KEYWORDS

Carboxymethyl cellulose;
Nanocomposite;
Lactic acid;
Anticancer;
Antioxidant;
Photocatalysis

Abstract In this paper, the microwave-assisted synthesis of carboxymethyl cellulose-cl-poly(lactic acid–co-itaconic acid)/ZnO-Ag nanocomposite [CMC-cl-p(LA-co-IA)/ZnO-Ag] has been discussed. Lactic acid (LA) and itaconic acid (IA) monomers were grafted onto carboxymethyl cellulose (CMC) using potassium persulphate and N, N'-methylene-bis-acrylamide (MBA) as initiator and crosslinker, respectively at optimized conditions of temperature and pressure. The nanocomposite was characterized using different techniques such as Fourier transform infrared spectroscopy (FTIR), field emission scanning electron microscopy (FESEM), transmission electron microscopy (TEM), X-ray diffraction (XRD), thermogravimetric analysis (TGA) and energy dispersive X-ray (EDX). XRD, TEM and FTIR spectral analysis confirmed the formation of the nanocomposite. The release of amoxicillin drug-using nanocomposite as a function of pH and time has been investigated. The maximum drug release of 94.64% was pragmatic at pH 2.2 after 6 h. The degradation of congo red using nanocomposite followed the pseudo-first-order reaction model with the regression coefficient (R^2) values of 0.99312. The nanocomposite was also explored for anticancer behavior against yeast cells.

* Corresponding authors.
E-mail addresses: dpathania74@gmail.com (D. Pathania), vinodfcy@gmail.com (V.K. Gupta).
Peer review under responsibility of King Saud University.

Production and hosting by Elsevier

https://doi.org/10.1016/j.arabjc.2020.07.001
1878-5352 © 2020 Published by Elsevier B.V. on behalf of King Saud University.
This is an open access article under the CC BY-NC-ND license (http://creativecommons.org/licenses/by-nc-nd/4.0/).

Contents

1. Introduction . . . 6967
2. Materials and methods . . . 6968
2.1. Materials . . . 6968
2.2. Synthesis of CMC-cl-p(LA-co-IA)/ZnO-Ag nanocomposite . . . 6968
2.2.1. Synthesis of ZnO/Ag nanocomposite . . . 6968
2.2.2. Preparation of CMC-cl-p(LA-co-IA)/ZnO-Ag nanocomposite . . . 6968
2.3. Characterization . . . 6968
2.3.1. Fourier transform infrared (FTIR) spectroscopy . . . 6968
2.3.2. Field emission scanning electron microscopy (FESEM) . . . 6968
2.3.3. Transmission electron microscopy (TEM) . . . 6969
2.3.4. X-ray diffraction (XRD) . . . 6969
2.3.5. Thermogravimetric (TGA/DTA/DSC) analysis . . . 6969
2.3.6. Energy dispersive X-ray (EDX) studies . . . 6969
2.3.7. Anticancer activity of the CMC-cl-p(LA-co-IA)/ZnO-Ag nanocomposite . . . 6969
2.3.8. Drug delivery . . . 6969
2.3.9. Photocatalysis using nanocomposite . . . 6969
3. Results and discussion . . . 6970
3.1. Characterisations . . . 6970
3.1.1. FTIR spectra of CMC-cl-p(LA-co-IA)/ZnO-Ag nanocomposite . . . 6970
3.1.2. SEM analysis . . . 6970
3.1.3. TEM analysis . . . 6970
3.1.4. X-ray diffraction (XRD) . . . 6970
3.1.5. Thermal curves . . . 6970
3.1.6. Energy dispersive X-ray (EDX) studies . . . 6970
3.1.7. Anticancer activity of CMC-cl-p(LA-co-IA)/ZnO-Ag nanocomposite . . . 6971
3.1.8. Drug delivery . . . 6971
3.1.9. Photocatalysis by the CMC-cl-p(LA-co-IA)/ZnO-Ag nano composite . . . 6972
4. Conclusion . . . 6974
Acknowledgments . . . 6974
References . . . 6974

1. Introduction

Nanotechnology is emerging as a rapidly growing field for the manufacturing of new materials (Albrecht et al., 2006). Nano molecules have well-defined chemical, mechanical, and optical properties. Nanocomposites are multiphase materials with one of the components present in the nanoscale. Since most of the hydrogels derived from synthetic polymers are not environment friendly, so there is an emerging need to use natural biopolymers to fabricate hydrogels and nanocomposite for diverse applications. Cellulose and its derivatives having crystalline and fibrous structures are extensively used to synthesize nanocomposites with significant biomedical applications (Giammona et al., 1999; Krogars et al., 2000). Many attempts for the modifications of biopolymers either by grafting to form hydrogel or by combining them with metal/metal oxide nanoparticles have been reported (Ding et al., 2011). Nanocomposites obtained from hydrogels have been extensively used in photocatalysis, antibacterial, drug delivery, and tissue engineering (Diwakar and Rajat, 2010; Gupta et al., 2015). In recent years, organic/inorganic nanocomposite containing biopolymer and metal ions have been synthesized. The biopolymer-based nanocomposites are preferred because they are cheap, renewable, and available in excess. The primary advantage of grafted polysaccharide is to formulate compound with desired drug release. Drug delivery systems have improved therapy periods of drug activity, appropriate routes of administration, and improved site-specific delivery to reduce the undesirable adverse effects. The literature studies have revealed the formation and stability of nanocomposite and microbeads for the targeted release of anticancer drugs (Sun et al., 2020; Sun et al., 2019a; Sun et al., 2019b).

Biopolymers are chemical modifications due to their unique properties such as biodegradability, nontoxic, economic nature, and bio-compatibility. Polymers possess large numbers of hydroxyl groups which form complex with metal ions and afford good milieu for the growth of semiconductor nanoparticles. They have been used to encapsulate the proteins and peptides. A majority of natural polymer-based drug delivery systems are either protein (collagen, gelatin, and albumin) or polysaccharide (starch, dextran, hyaluronic acid, pectin, and chitosan). The properties like high cost, low elasticity, and possible occurrence of an antigenic response have limited the degree of protein drugs. The modification of pH-sensitive functional groups such as $-CONH_2$, $-COOH/CH_3$, $-NH_2$, and SO_3H has made their use in the controlled release of drugs.

Carboxymethyl cellulose (CMC) is very important in food, textile, paper, paint, pharmaceutical, and cosmetic processing. It is a natural, non-toxic, and degradable biopolymer. Cellulose polyacrylamide nanocomposite has been effectively used for photocatalytic degradation of methylene blue dye (Zhou et al., 2014). The cellulose and its different derivatives are biocompatible (Shukla et al., 2013).

Itaconic acid is an unsaturated organic acid having various industrial applications. The polymeric esters of itaconic acid have been used in plastics, adhesives, and coatings. Many hydrogels have been reported using itaconic acid as monomers (Lanthong et al., 2006; Koetting and Peppas, 2014). Itaconic acid has two —COOH groups and hence a very small amount is required for making pH-sensitive hydrogel.

Lactic acid is an aliphatic biodegradable acid obtained from renewable sources, is gaining more interest in recent years (Edlund et al., 2005; Slivniak and Domb, 2005; Chen et al., 2005). Polylactic acid has many biomedical applications due to its biocompatible and biodegradable nature (Nouvel et al., 2004; Gupta et al., 2016). The use of lactic acid has provided more active sites for the binding of drugs (Ikada and Tsuji, 2000).

Zinc oxide nanoparticles synthesized by the green method showed antimicrobial and antioxidant properties (El-Sayed et al., 2020). Noble metal cations doped on films of CMC/PVA/Zeolite displayed excellent biological properties (Youssef et al., 2019). Literature studies further show that nanocomposites involving synthetic and natural polymers eco-friendly showed excellent antibacterial and optical properties (Youssef et al., 2017a; Youssef et al., 2017b; Noah et al., 2017; El-Nahrawy et al., 2016; Moustafa et al., 2019)

Nanosized metal oxide with suitable band gaps is effectively used for the removal of toxic organic pollutants from aqueous systems (Zhao et al., 2015; Jing et al., 2013; He et al., 2013). Zinc oxide (ZnO) is one of the most commonly used metal oxides. It is cheap, non-toxic, environment friendly. It has a suitable bandgap of 3.37 eV (Wang et al., 2011; Li et al., 2011). Many efforts have been attempted to improve the photocatalytic activity of ZnO in visible light which depends upon the inhibition of the electron-hole recombination process. This can be achieved by doping ZnO either with metals or non-metals (Ansari et al., 2013; Ullah and Dutta, 2008; Han et al., 2012; Jiang et al., 2008; Shinde et al., 2012; Qiu et al., 2008). The use of noble metals for doping has further increased the corrosion resistance. The ZnO based nanocomposites have found enhanced photocatalytic efficiency. Metal-ZnO nanocomposite has a higher surface to volume ratio than conventional materials. Out of different noble metals, silver metal is of great interest due to its ability to augment the photocatalysis along with antibacterial properties (Zhang et al., 2012; Duan et al., 2006; Xie et al., 2010; Pathania et al., 2015).

In the present work, carboxymethyl cellulose-cl-poly(lactic acid–co-itaconic acid)/ZnO-Ag nanocomposite has been discussed. The nanocomposite was characterized using Fourier transform infrared spectroscopy (FTIR), field emission scanning electron microscopy (FESEM), transmission electron microscopy (TEM), X-ray diffraction (XRD), thermogravimetric analysis (TGA) and energy dispersive X-ray (EDX). The release of amoxicillin drug-using nanocomposite has been investigated. Their potential roles in photocatalysis, drug delivery, and anticancerous behavior of nanocomposite have been explored.

2. Materials and methods

2.1. Materials

All chemicals used in this study were of analytical grade carboxymethyl cellulose (CMC), lactic acid (LA), itaconic acid (IA), potassium persulfate (KPS), zinc nitrate, N,N'-methylene-bis-acrlymaide (MBA) and sodium hydroxide were purchased from Loba Chemie Pvt. Ltd., India. Amoxicillin, silver nitrate, and sodium borohydride were obtained from Himedia Pvt. Ltd., India. All glassware used during experiments were cleaned thoroughly and rinsed with acetone before use. All the solutions were prepared in double-distilled water.

2.2. Synthesis of CMC-cl-p(LA-co-IA)/ZnO-Ag nanocomposite

2.2.1. Synthesis of ZnO/Ag nanocomposite

Ag/ZnO nanoparticles were synthesized using the co-precipitation method. In this method, 50.0 mL of 0.1 M zinc nitrate solution was stirred at about 40–50 °C. To the above solution 40 mL of 0.1 M sodium hydroxide was added dropwise with constant stirring till turbidity appeared. This mixture was stirred for one hour on the magnetic stirrer. In another beaker, 25 mL of 0.1 M silver nitrate was stirrer for half an hour at 40–50 °C. It was followed by the addition of 50 mL of 0.1 M sodium borohydride solution dropwise with stirring till the formation of precipitates of silver. Now mixed these precipitates into the mixture prepared in the first beaker. The resultant mixture was stirred for 2 h at 60 °C. It was then cooled and filtered. The obtained precipitates were dried at 50 °C in hot air for 12 h.

2.2.2. Preparation of CMC-cl-p(LA-co-IA)/ZnO-Ag nanocomposite

CMC-cl-p(LA-co-IA)/ZnO-Ag nanocomposite was synthesized by the coprecipitation method using microwave radiations. In this method, in the first beaker 0.5 gm of CMC was dissolved in 10.0 mL of double-distilled water. It was followed by the addition of 0.3 gm of potassium persulphate with continuous shaking. In another beaker 0.05 gm of MBA was added into the mixture of 1.0 gm of IA and 2.0 mL of LA. The above mixtures taken in two different beakers' solutions were mixed and stirred for 10 min. It was followed by the addition of ZnO/Ag powder prepared above in Section 2.2.1 with shaking. The resultant mixture was exposed to microwave radiations at 100 W for 3 min. The mixture was kept for 24 h undisturbed to complete the process of hydrogel formation. The obtained precipitates were washed with double distilled water and acetone. The final precipitates were filtered and dried in a hot air oven at 60 °C. The nanocomposite was then powdered and stored for further studies.

2.3. Characterization

2.3.1. Fourier transform infrared (FTIR) spectroscopy

CMC-cl-p(LA-co-IA)/ZnO-Ag nanocomposite was characterized by Fourier transform infrared (FTIR) spectroscopy for the structure and functional group present in it (Pathania et al., 2012). An FTIR spectrum was recorded in the region between 400 and 4000 cm^{-1}. The FTIR spectrum was obtained using a spectrophotometer (Perkin Elmer Spectrum-BX USA).

2.3.2. Field emission scanning electron microscopy (FESEM)

FESEM analysis was used to analyze the surface morphology of nanocomposite. The morphological images of the nanocomposite were obtained using Nova Nano SEM 450 (FEI Technai) scanning electron microscope. The micrographs of samples were recorded at different magnifications.

2.3.3. Transmission electron microscopy (TEM)

Transmission electron microscopy (TEM) was used to study the anatomy of nanocomposites. In this analysis, the sample was prepared by dispersing 2–3 drops of (1 mg/mL) nanocomposite solution into a 3 mm copper grid and dried at ambient temperature. Transmission electron microscopy was used to study the size of particles. It was studied by transmission electron microscope (FEI 200 KvTecnai) using an accelerating voltage of 15 kV.

2.3.4. X-ray diffraction (XRD)

X-ray diffraction is a non-destructive analytical technique used for the identification and quantitative analysis of various crystalline forms of molecules. This technique is used for the characterization and identification of polycrystalline phases. XRD analysis of nanocomposite was attempted using a Model D/Max-2500Pc X-ray diffractometer.

2.3.5. Thermogravimetric (TGA/DTA/DSC) analysis

The thermal analysis technique was used to determine the physical changes in the substance when subjected to a controlled temperature program. TGA is very helpful to study the effect of temperature on the stability and behavior of a substance (Yang et al., 2014). In this technique, nanocomposites were heated in a nitrogen atmosphere in the temperature ranging from 50 °C to 750 °C.

2.3.6. Energy dispersive X-ray (EDX) studies

Energy-dispersive X-ray was used to confirm the elemental constituents and purity of the nanocomposite. Moreover, the atomic ratio obtained after the analysis confirmed the stoichiometric ratio of the elements present in the nanocomposite.

2.3.7. Anticancer activity of the CMC-cl-p(LA-co-IA)/ZnO-Ag nanocomposite

Yeast cells were used to calculate the anticancer behavior of nanocomposites. *Saccharomyces cerevisiae* strain *tsa1*Δ(*MAT*a *his3*Δ*1 leu2*Δ*0 met15*Δ*0 ura3*Δ*0tsa1*: *KAN*) was used, in which the TSA1 gene was deleted using kanamycin cassette (Wong et al., 2002). To analyse the effect of CMC-cl-p(LA-co-IA)/ZnO-Ag nanocomposite nanoparticle, *tsa1*Δ yeast cells (OD_{600} 0.05) in YPD (2% yeast extract, 1% peptone and 2% dextrose in H_2O) liquid medium was treated with CNC nanoparticle at different concentration 0.25 mg/ml, 0.5 mg/ml and 1 mg/ml for 16 h at 30 °C on shaking. Later cells were harvested and washed with water and serial dilutions of the equal number of cells were spotted on YPD or YPD agar media containing 2 mM H_2O_2.

2.3.8. Drug delivery

2.3.8.1. Drug loading. The loading of amoxicillin drug was carried out by immersing 100 mg of nanocomposite in the form of pellets into 100 mL of 100 ppm amoxicillin solution. The drug loading was optimized for different physiological conditions at 24 °C. The concentration of the drug was determined by taking out 3 mL of supernatant solution and recording the absorbance using a double beam UV–Vis spectrophotometer. The drug loading efficiency of CMC-cl-p(LA-co-IA)/ZnO-Ag was calculated using the following formula:

$$\text{Percentage of drug loading} = \frac{\text{Total amount of drug} - \text{Free drug}}{\text{Total amount of drug}} \times 100$$

Since the drug loading was found maximum in distilled water hence it was selected for further loading studies.

2.3.8.2. Drug release studies. Drug release of nanocomposite hydrogel mainly depends on the swelling behavior of the hydrogel and interaction of the drug with the polymers and the solubility of the drug in the release media (Brazel and Peppas, 1999). The drug release by CMC-cl-p(LA-co-IA)/ZnO-Ag was studied at different physiological conditions like double distilled water, simulated gastric fluid (SGF) (pH 2.2) and simulated gastrointestinal fluid (SIF) i.e. at pH 7.4 and pH 9.4. To study the drug release, amoxicillin loaded dried nanocomposite were added into 100 mL each of double-distilled water, SGF (pH 2.2), SIF (pH7.4), and 9.4 pH solutions. The 3 mL test sample was withdrawn at different time intervals and absorbance was noted using UV–Vis spectrophotometer. All drug release studies were performed in triplicate and the means of all measurements were calculated. The results were presented in terms of cumulative percentage release. The drug release in water was found to be least because of the stability of the nano composite-drug complex. The percentage of drug release was calculated by using the formula as (Pathania et al., 2016):

$$\text{Percentage drug release} = \frac{\text{Amount of drug released}}{\text{Amount of drug loaded}} \times 100$$

2.3.8.3. Kinetics of drug release. A mathematical model was used to study the drug release behavior of nanocomposite (Brannon-Peppas and Peppas, 1989; Khare and Peppas, 1993; Alfrey et al., 1966). The drug release behavior was described using the generalized empirical equation. The liquid uptake of the sample is described by following empirical Eq. As follow:

$$M_s = k\,t^n$$

where 'k' and 'n' are constants. 'n' = 0.5 reveals the normal Fickian diffusion and the value of 'n' = 1.0 signifies case II diffusion. The value of 'n' lies between 0.5 and 1.0 for anomalous diffusion (Ritger and Peppas, 1987a). The drug release mechanism of the drug was evaluated using the following Eq. (Ritger and Peppas, 1987b):

$$M_t/M_\infty = k\,t^n$$

where M_t/M_∞ is the fraction of drug released at time t and ∞, respectively, k is the apparent release rate constant, and n is the diffusion exponent. The value of n determines the nature of the release mechanism. The equation represents pure diffusion or Fickian controlled drug release if the value of n is 0.5. The value of n = 1 represents the swelling controlled drug release or case II transport which is non-Fickian and for other values, the release mechanism is abnormal i.e. a combined mechanism of pure diffusion and case II transport will be operating (Lin and Metters, 2006).

2.3.9. Photocatalysis using nanocomposite

Congo red (CR) ($C_{32}H_{22}N_6Na_2O_6S_2$, molecular weight: 696.67) was used as a model dye to investigate the photocat-

alytic activity of CMC-cl-p(LA-co-IA)/ZnO-Ag nanocomposite. In this, 50 mg of the CMC-cl-p(LA-co-IA)/ZnO-Ag nanocomposite was added into 50 mL of CR solution of 30 mg/L ion concentration in the beaker. The above mixture was magnetically stirred for 60 min in dark and then the beaker was kept in the light. Another set containing the same was directly kept in the sunlight. The changes in the concentration of both the solutions were recorded at 498 nm by using a spectrophotometer. The % degradation was calculated using the following equation (Kansiz et al., 1999):

$$\%\ degradation = \frac{C_0 - C_t}{C_t} \times 100$$

where C_o is initial absorbance and C_t is the absorbance at any time

Further, to calculate the reaction rate of photodegradation, pseudo-first-order kinetics were applied by plotting the values of log A_0/A with time and the rate constant was calculated as

$$k = 2.303 \times slope$$

where the slope is obtained from the plot of log A_0/A and t.

3. Results and discussion

3.1. Characterisations

3.1.1. FTIR spectra of CMC-cl-p(LA-co-IA)/ZnO-Ag nanocomposite

Fig. 1 (a-c) shows the FTIR spectra of carboxymethyl cellulose (CMC), hydrogel, and its nanocomposite. The presence of a strong absorption band at 3162 cm^{-1} indicated —OH bond stretching vibration in the nanocomposite. A peak at 2961 cm^{-1} was assigned due to —C—H stretching of $—CH_2$ group (Liu et al., 2015). Another peak at 2343 cm^{-1} was due to overtones and combinations of —OH bending and —C—O stretching vibrations (Singh and Sharma, 2017). The peak at 1710 cm^{-1} was assigned to —C═O stretching in the nanocomposite introduced due to LA and IA. A band at 1568 cm^{-1} was due to ring stretching of glucose. Another band around 1368 cm^{-1} was assigned to —OH bending vibrations. The appearance of peaks at 1098 cm^{-1} and 1021 cm^{-1} may be due to —C—O and —C—O—C stretching vibrations of ether and alcoholic groups. An absorption band absorbed at 785 cm^{-1} showed the presence of a pyranose ring in the hydrogel (Prashar et al., 2012). An absorption peak recorded at 603 cm^{-1} was due to the presence of Ag and Zn in CMC-cl-p(LA-co-IA)/ZnO-Ag.

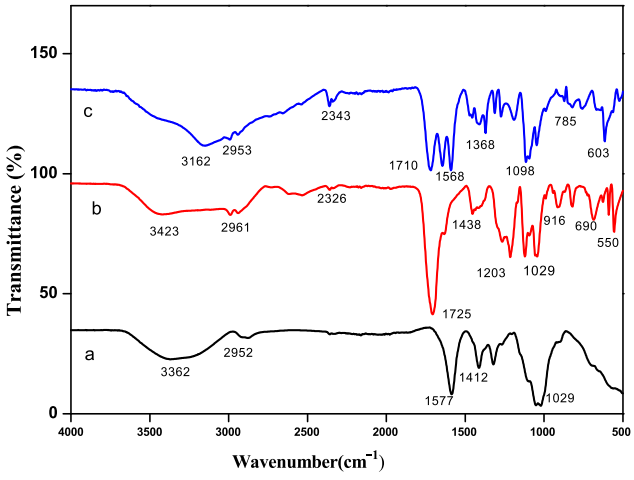

Fig. 1 FTIR spectra of (a) carboxymethyl cellulose (b) GCP hydrogel and (c) GCP/ZO-S nano composite.

3.1.2. SEM analysis

SEM images of CMC-cl-p(LA-co-IA) hydrogel and its nanocomposites were reported in Fig. 2(a-b). The images shows the particles of enough size diversity. The surface morphology of nano composite was found to be rough, porous, and heterogeneous compared to smooth surface of carboxymethyl cellulose. The surface of the hydrogel clearly showed two different shaped structures. The shining rod-shaped particles correspond to ZnO and spherical particles attached on the surface indicated Ag.

3.1.3. TEM analysis

TEM images of the nano composites were reported in Fig. 2(c–d). The particles can be easily classified into two different groups by different shapes and sizes. As silver has a higher atomic number, it shows a greater contrast than ZnO. So, the darker particles in Fig. 2(c) were assigned to silver while the lighter corresponds to ZnO. The particles with small agglomerates nearly have spherical shapes. Two different contrast fringes can be found in the boundary of the Ag nanoparticle Fig. 2(d). The indistinct grain boundary of the Ag nanoparticle is seen due to diffusion contact with ZnO. This confirmed the formation of Ag/ZnO nanoparticles. The particle size of the Ag nanoparticle embedded in the hydrogel was in found in the range from 15 to 20 nm.

3.1.4. X-ray diffraction (XRD)

XRD pattern of CMC-cl-p(LA-co-IA)/ZnO-Ag nanocomposites was demonstrated in Fig. 3. The broad peaks at 2θ value of 20-30° were assigned to a polymeric network of carboxymethyl cellulose. Peaks at 21.42, 23.34, and 26.8°where corresponds to the partial crystalline structure of CMC. A definite line broadening of the XRD peaks indicates that the prepared material consists of particles in the nanoscale range. The peaks at 38.33°, 44.40°, and 64.49°corresponds to (111), (200) and (220) planes indicating cubic crystalline face structure of silver nanoparticles (Prakash et al., 2013). The diffraction peaks located at 31.63°; 34.4°, and 35.37° associated to (100), (002) and (101) planes of ZnO nanoparticles (Lu et al., 2017; Sood et al., 2017).

3.1.5. Thermal curves

The effect of temperature on the stability of CMC-cl-p(LA-co-IA)/ZnO-Ag nanocomposite is presented in Fig. 4. It was seen that nanocomposite first loses weight with a rise in temperature. This weight loss may be due to loss of moisture upon heating. Upon further increase in temperature, the gradual decrease in weight was observed. This weight loss was very slow which indicates the stability of the nanocomposite.

3.1.6. Energy dispersive X-ray (EDX) studies

EDX spectrum (Fig. 5) of CMC-cl-p(LA-co-IA)/ZnO-Ag nanocomposite revealed a strong signal of the silver and zinc (two peaks each). In the analysis elemental ratio of Ag

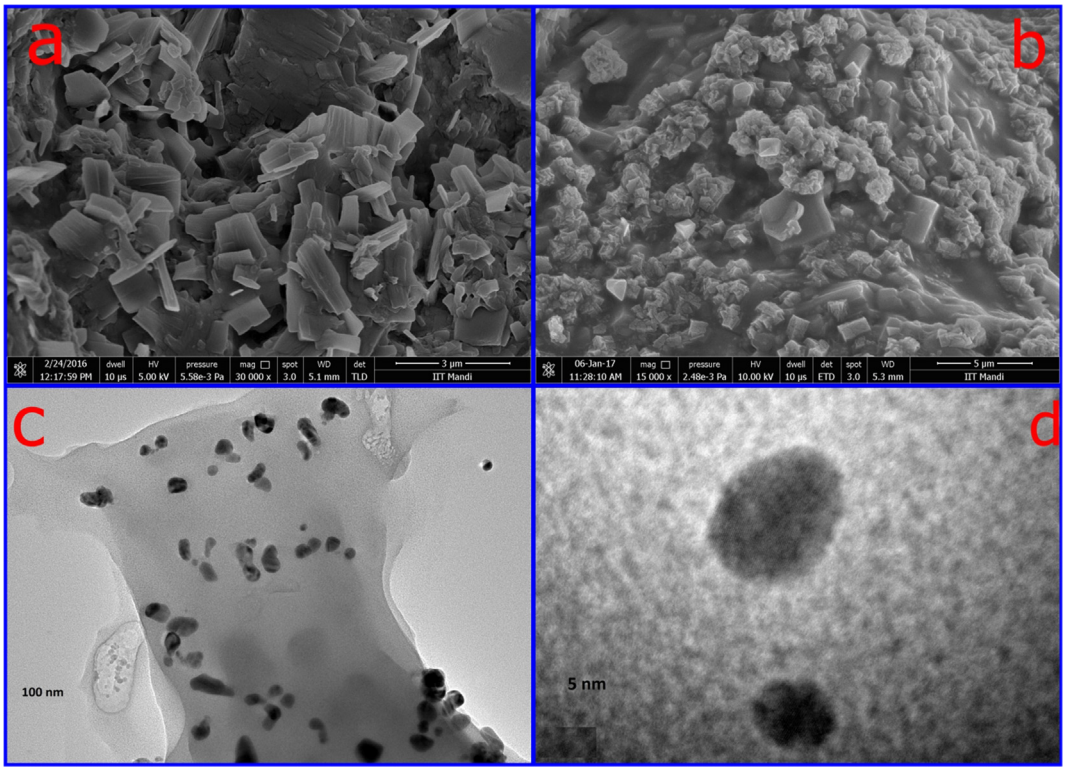

Fig. 2 SEM images of (a) GCP (b) GCP/ZO-S nano composite and (c-d) TEM images of GCP/ZO-S nano composite.

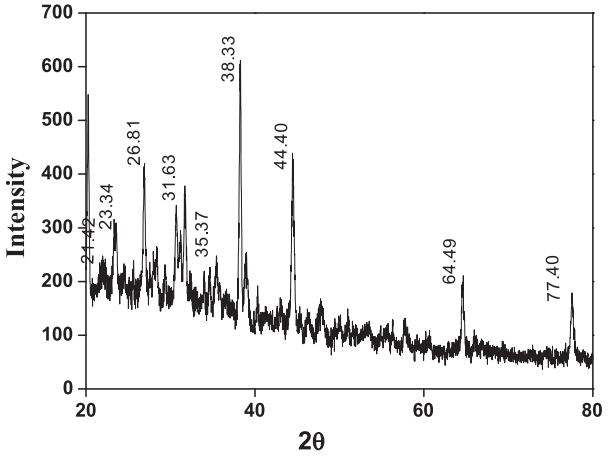

Fig. 3 XRD spectra of GCP/ZO-S nano composite.

(0.28%) and Zn (0.24%), the present was very close to their molar ratio (1:1) used during their preparation. EDX profile also showed weak oxygen peaks arises from the biomolecules that were bound to the surface of nanocomposite indicating the reduction of silver ions to elemental silver. Another peak corresponding to Cu in the EDX was due to the Cu grid on which the sample was coated. All these peaks in EDX confirmed the formation of Ag/ZnO based nanocomposites.

3.1.7. Anticancer activity of CMC-cl-p(LA-co-IA)/ZnO-Ag nanocomposite

Fig. 6 shows the anticancer activity of CMC-cl-p(LA-co-IA)/ZnO-Ag nanocomposite. It has been observed that redox-mediated apoptosis of cancer cells using anti-cancer drugs or chemotherapy decreased by redox scavenging activity of cellular antioxidants (Trzeciecka et al., 2016). Yeast cells lacking *tsa1* gene were sensitive to oxidative stress and using this property we looked for the effect of CMC-cl-p(LA-co-IA)/ZnO-Ag nanocomposite on normal cells and oxidatively stressed cells. Indicated cells in Fig. 6 were grown in YPD medium with CMC-cl-p(LA-co-IA)/ZnO-Ag nanocomposite for 16-hour serial dilutions of grown cells were spotted on YPD or YPD agar media with 2 mM H_2O_2. It was indicated that CMC-cl-p(LA-co-IA)/ZnO-Ag nanocomposite is not toxic to the unexposed cells.

It showed dramatic effects in exacerbating the effects of H_2O_2. We found that cells are completely dead in the presence of H_2O_2 at 1 mg/ml concentration. Since high expression of peroxide quenching enzymes leads to the development of cancer CMC-cl-p(LA-co-IA)/ZnO-Ag nanocomposite could be an answer to further induce apoptosis in the cells.

3.1.8. Drug delivery

3.1.8.1. Drug loading. The loading efficiency of nanocomposite using amoxicillin drug was studied in four different physiological conditions (Pathania et al., 2016). The drug loading of 54%, 49%, and 42% was obtained at pH 2.2, 7.4, and 9.4, respectively after 24 h. The maximum drug loading of 56% was observed in distilled water.

3.1.8.2. Cumulative drug release. Cumulative drug release of amoxicillin was studied using CMC-cl-p(LA-co-IA)/ZnO-Ag nanocomposite at different physiological conditions like double distilled water, simulated gastric fluid (pH 2.2) and simulated gastrointestinal fluid (pH 7.4, pH 9.4). The results

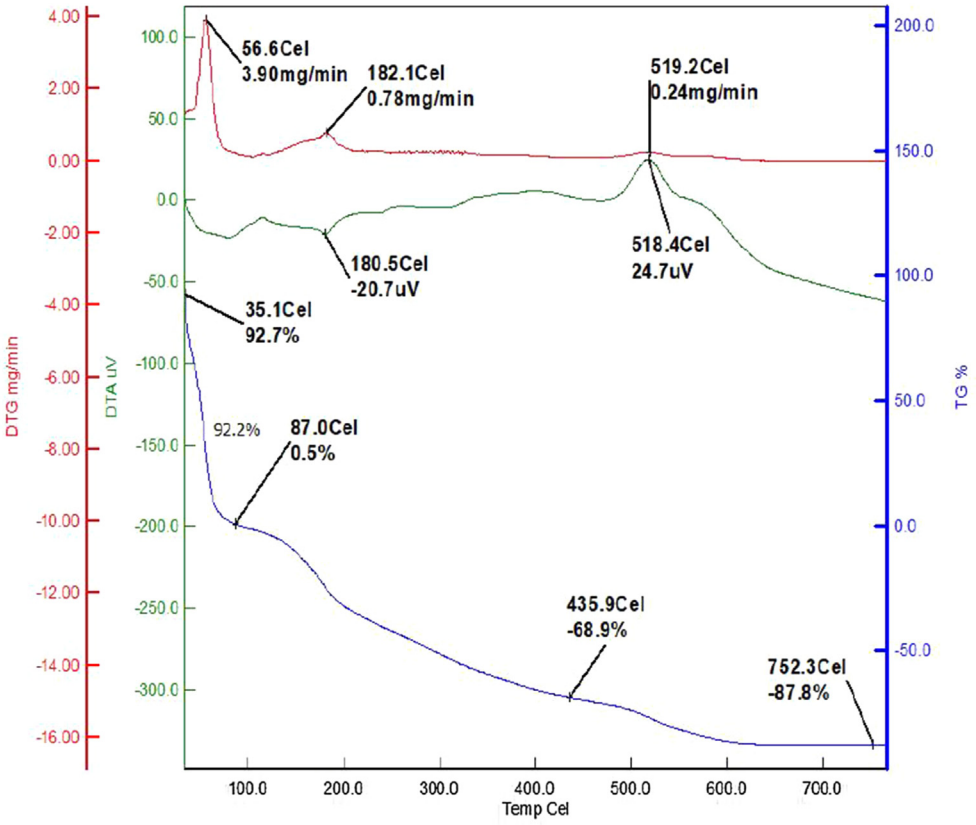

Fig. 4 Thermal stability curves of GCP/ZO-S nano composite.

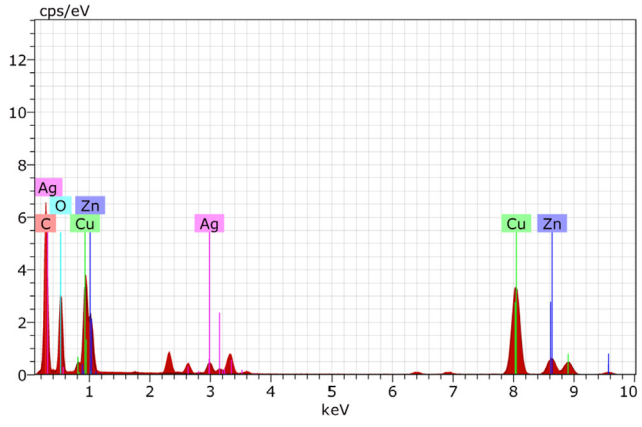

Fig. 5 EDX spectra of GCP/ZO-S nano composite.

of cumulative drug release were shown in Fig. 7 (a). It was observed that the initial release of drugs was faster and decrease with time. It may be due to the reason that initially the drug nearer to the surface was released faster than the drug incorporated deeply (Liu et al., 2008). From the graph, it was recorded that 71.43% of loaded amoxicillin was released within the first three hours of administration at pH 2.2. The mathematical treatment of drug release (Fig. 7 (b)) showed non Fickian release. The mechanism of drug loading and drug release using nano composite is shown in scheme 1.

3.1.9. Photocatalysis by the CMC-cl-p(LA-co-IA)/ZnO-Ag nano composite

CMC-cl-p(LA-co-IA)/ZnO-Ag nanocomposite was investigated for the photocatalytic degradation of congo red at different time intervals. Fig. 8 (a) described the adsorption of congo red in dark (1 h) followed by degradation in sunlight (3 h) whereas Fig. 8(b) showed the degradation directly in sunlight. In the dark about 14% degradation (60 min) was observed. It increases to 92.47% in the presence of sunlight (next 180 min). It was further noted that direct exposure to sunlight for 240 min degraded the dye to 93.19%. Moreover, with an increase in the irradiation time, there was an increase in degradation of dye. The CMC-cl-p(LA-co-IA)/ZnO-Ag can photodegrade congo red dye due to the presence of Ag and ZnO nanoparticles which generated electron-hole pairs leading to the formation of free radicals that disrupted the conjugation of dye molecules (Pathania et al., 2014).

The degradation of dye may be due to reactive oxidizing species (O_2*, OH*) which were generated by simultaneous reactions. The kinetics of congo red degradation showed a linear correlation with time as shown in Fig. 8 (c). The photodegradation of congo red by nanocomposite follows pseudo-first-order kinetics. When a graph of log A_0/A and time was plotted for adsorption + photocatalysis Fig. 8(c) and direct photolysis Fig. 8(d), we got reaction rate constant

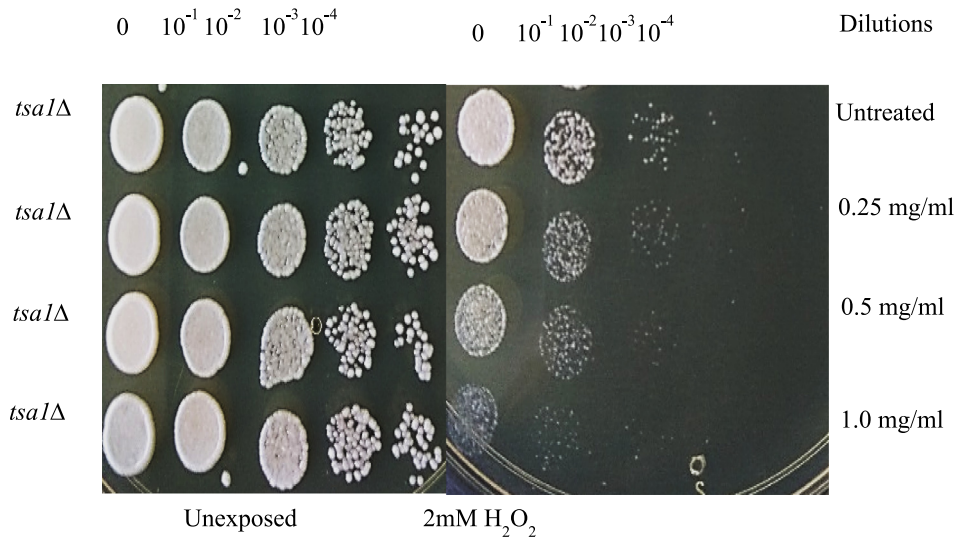

Fig. 6 The behaviour of exposed and unexposed yeast cells to different concentrations of GCP/ZO-S nano composite.

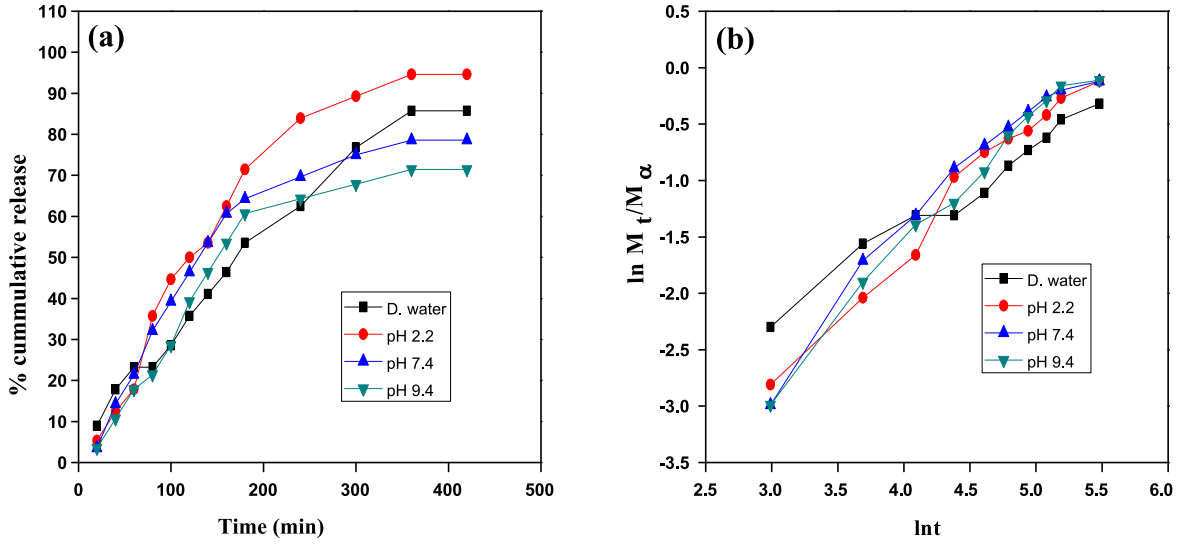

Fig. 7 Drug delivery study (a) % cumulative release and (b) kinetics of the drug release by the GCP/ZO-S nano composite.

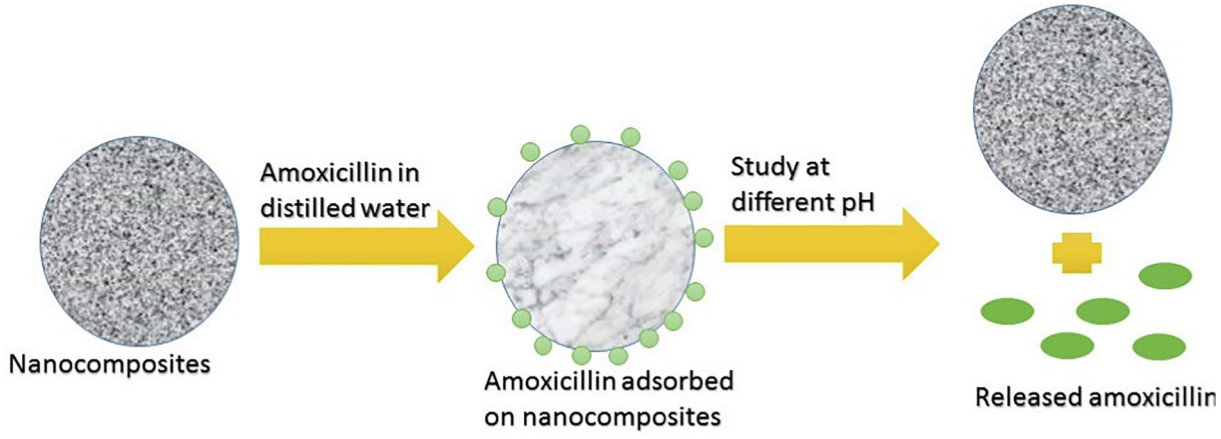

Scheme 1 Mechanism of drug loading and drug release using CMC-cl-p(LA-co-IA)/ZnO-Ag nano composite.

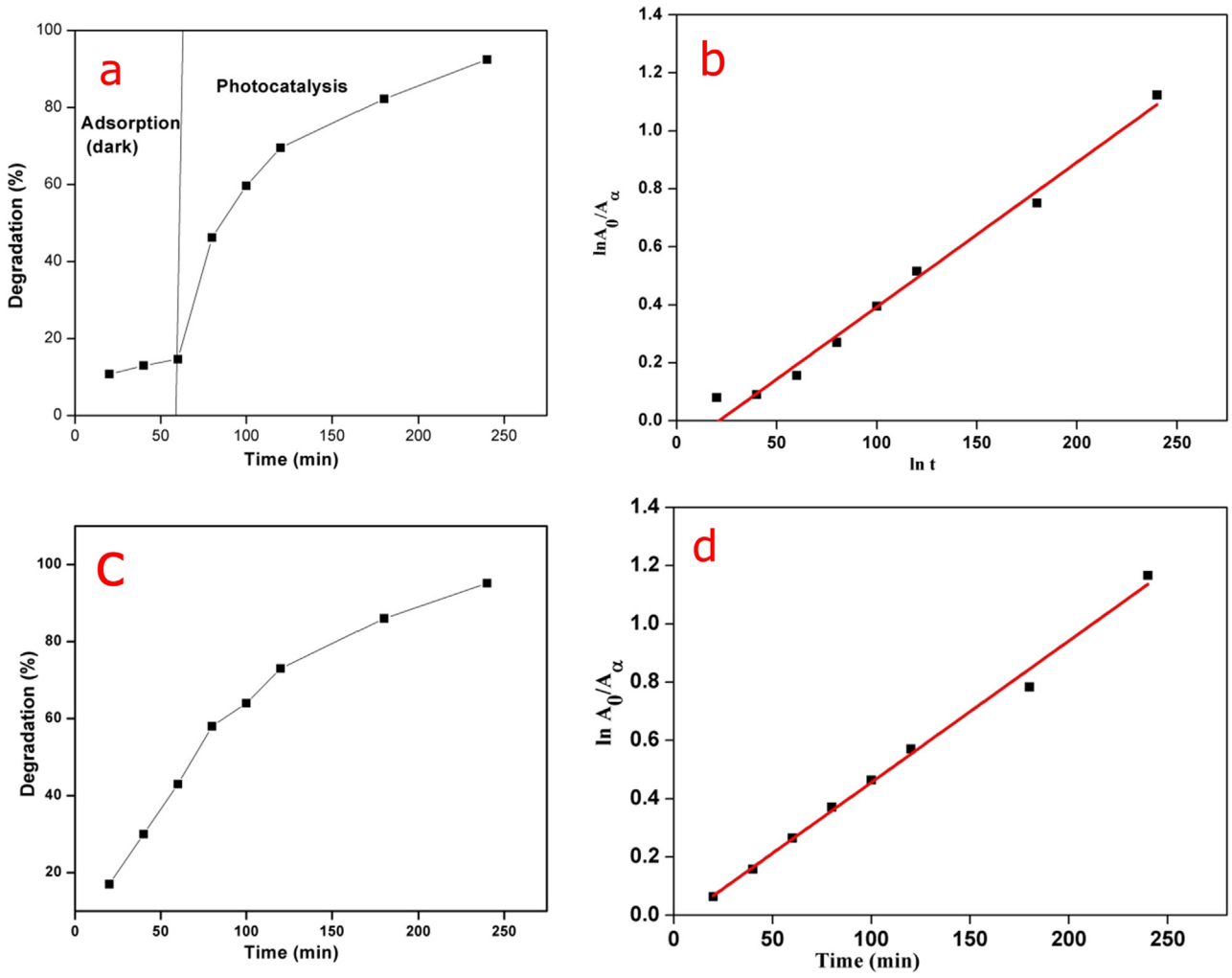

Fig. 8 Photocatalysis by GCP/ZO-S nano composite (a) % degradation in adsorption followed by photocatalysis (b) Pseudo first order kinetic of adsorption followed by photocatalysis (c) % degradation in direct sunlight (d) Pseudo first order kinetic in direct sunlight.

values of 0.01149 min^{-1} and 0.01119 min^{-1} with regression coefficient (R^2) values of 0.98889 and 0.99312, respectively.

4. Conclusion

Microwave-assisted green synthesis for the preparation of CMC-cl-p(LA-co-IA)/ZnO-Ag nanocomposite was presented in this paper. TEM images of CMC-cl-p(LA-co-IA)/ZnO-Ag showed nanoparticles in the range between 10 nm and 25 nm. Further, the XRD analysis confirmed the crystalline nature of nano composite. The EDX analysis of the nanocomposite established the presence of the elemental silver and zinc and no peaks for impurities. CMC-cl-p(LA-co-IA)/ZnO-Ag nanocomposite was also studied for the controlled release of amoxicillin at various pH prevailing in the gastrointestinal tract. The maximum drug release of 94.64% was observed at pH 2.2 after 6 h, The drug release rate was found higher in acidic pH. The nano composite was also studied for the photodegradation of congo red dye with a high degree of efficiency. Maximum degradation of 93.2% was observed after 4 h of photocatalysis directly in the sunlight. Experimental results indicated that prepared CMC-cl-p(LA-co-IA)/ZnO-Ag nanocomposite has great potential for an effective role in drug delivery and photodegradation.

Acknowledgments

We all are thankful to the Central University of Jammu and Shoolini University for providing us all the necessary chemicals, equipment, and the help needed during the entire project work. We are also thankful to IIT, Mandi (H.P.) and NIT Jalandhar (Punjab) for the characterizations of samples. This research did not receive any specific grant from funding agencies in the public, commercial, or not-for-profit sectors.

References

Albrecht, M.A., Cameron, W.E., Colin, L.R., 2006. Green chemistry and the health implications of nanoparticles. Green Chem. 8, 417–432.

Giammona, G., Pitarresi, G., Cavallaro, G., Spadaro, G., 1999. New biodegradable hydrogels based on an acryloylated polyaspartamide cross-linked by gamma irradiation. J. Biomater. Sci. Polym. Ed. 10, 969–987.

Krogars, K., Heinämäki, J., Vesalahti, J., Marvola, M., Antikainen, O., Yliruusi, J., 2000. Extrusion–spheronization of pH-sensitive

polymeric matrix pellets for possible colonic drug delivery. Int. J. Pharm. 199, 187–194.
Ding, S., Wang, Y., Hong, Z., Lü, X., Wan, D., Huang, F., 2011. Biomolecule-Assisted Route to Prepare Titania Mesoporous Hollow Structures. Chem.-a Eur. J. 17, 11535–11541.
Diwakar, T., Rajat, K., 2010. Performance studies for floating tablet of ofloxacin. Int. J. Pharm. & Life Sci. 1, 419–442.
Gupta, D., Singh, D., Kothiyal, N.C., Saini, A.K., Singh, V.P., Pathania, D., 2015. Synthesis of chitosan-g-poly (acrylamide)/ZnS nanocomposite for controlled drug delivery and antimicrobial activity. Int. J. Biol. Macromol. 74, 547–557.
Sun, X., Pan, C., Ying, Z., Dongyan, Y.u., Duan, X., Huang, F., Ling, J., 2020. Xiao-kun, Ouyang Stabilization of zein nanoparticles with k-carrageenan and tween 80 for encapsulation of curcumin. Int. J. Biol. Macromol. 146, 549–559.
Sun, Xiaoxiao, Liu, Chao, Omer, A.M., Yang, Li-Ye, Ouyangm, Xiao-kun, 2019a. Dual-layered pH-sensitive alginate/chitosan/kappa-carrageenan microbeads for colon-targeted release of 5-fluorouracil. Int. J. Biol. Macromol. 132, 487–494.
Sun, Xiaoxiao, Liu, Chao, Omer, A.M., Wuhuan, Lu, Zhang, Shuxing, Jiang, Xun, Hongjie, Wu, Di, Yu, Ouyang, Xiao-kun, 2019b. pH-sensitive ZnO/carboxymethyl cellulose/chitosan bionanocomposite beads for colon-specific release of 5-fluorouracil. Int. J. Biol. Macromol. 128, 468–479.
Zhou, C., Wu, Q., Lei, T., Negulescu, I.I., 2014. Adsorption kinetic and equilibrium studies for methylene blue dye by partially hydrolyzed polyacrylamide/cellulose nanocrystal nanocomposite hydrogels. Chem. Eng. J. 251, 17–24.
Shukla, S., Nidhi, S., Pooja, N., Charu, A., Silvi, M., Rizwana, A.B., Dubey, G.C., Tiwari, A., 2013. Preparation and characterization of cellulose derived from rice husk for drug delivery. Adv. Mater. Lett. 4, 714–719.
Lanthong, P., Nuisin, R., Kiatkamjornwong, S., 2006. Graft copolymerization, characterization, and degradation of cassava starch-g-acrylamide/itaconic acid superabsorbents. Carbohydr. Polym. 66, 229–245.
Koetting, M.C., Peppas, N.A., 2014. pH-Responsive poly (itaconic acid-co-N-vinylpyrrolidone) hydrogels with reduced ionic strength loading solutions offer improved oral delivery potential for high isoelectric point-exhibiting therapeutic proteins. Int. J. Pharm. 471, 83–91.
Edlund, U., Källrot, M., Albertsson, A.C., 2005. Single-step covalent functionalization of polylactide surfaces. J. Am. Chem. Soc. 127, 8865–8871.
Slivniak, R., Domb, A.J., 2005. Lactic acid and ricinoleic acid based copolyesters. Macromolecules 38, 5545–5553.
Chen, G.X., Kim, H.S., Shim, J.H., Yoon, J.S., 2005. Role of epoxy groups on clay surface in the improvement of morphology of poly (L-lactide)/clay composites. Macromolecules 38, 3738–3744.
Nouvel, C., Dubois, P., Dellacherie, E., Six, J.L., 2004. Controlled synthesis of amphiphilic biodegradable polylactide-grafted dextran copolymers. J. Polym. Sci., Part A: Polym. Chem. 42, 2577–2588.
Gupta, V.K., Gupta, D., Agarwal, S., Kothiyal, N.C., Asif, M., Sood, S., Pathania, D., 2016. Fabrication of chitosan-g-poly (acrylamide)/Cu nanocomposite for the removal of Pb (II) from aqueous solutions. J. Mol. Liq. 224, 1319–1325.
Ikada, Y., Tsuji, H., 2000. Biodegradable polyesters for medical and ecological applications. Macromol. Rapid Commun. 21, 117–132.
El-Sayed, S.M., El-Sayed, H.S., Ibrahim, O.A., Youssef, A.M., 2020. Rational design of chitosan/guar gum/zinc oxide bionanocomposites based on Roselle calyx extract for Ras cheese coating. Carbohydr. Polym. 239, 116234.
Youssef, H.F., El-Naggar, M.E., Fouda, F.K., Youssef, A.M., 2019. Antimicrobial packaging film based on biodegradable CMC/PVA-zeolite doped with noble metal cations. Food Packaging and Shelf Life 22, 100378.
Youssef, A.M., Malhat, F.M., Abdel Hakim, A.A., 2017a. Imre Dekany. Synthesis and utilization of poly (methylmethacrylate) nanocomposites based on modified montmorillonite. Arabian J. Chem. 10, 631–642.
Youssef, A.M., El-Nahrawy, A.M., Abou Hammad, A.B., 2017b. Sol-gel synthesis and characterizations of hybrid chitosan-PEG/calcium silicate nanocomposite modified with ZnO-NPs and (E102) for optical and antibacterial applications. Int. J. Biol. Macromol. 97, 561–567.
Noah, A.Z., El Semary, M.A., Youssef, A.M., El-Safty, M.A., 2017. Enhancement of yield point at high pressure high temperature wells by using polymer nanocomposites based on ZnO & CaCO3 nanoparticles. Egypt. J. Pet. 26, 33–40.
El-Nahrawy, Amany M., Ali, Ahmed I., Abou Hammad, Ali B., Youssef, Ahmed M., 2016. Influences of Ag-NPs doping chitosan/calcium silicate nanocomposites for optical and antibacterial activity. Int. J. Biol. Macromol. 93, 267–275.
Moustafa, Hesham, Youssef, Ahmed M., Darwish, Nabila A., Abou-Kandil, Ahmed I., 2019. Eco-friendly polymer composites for green packaging: Future vision and challenges. Compos. B Eng. 172, 16–25.
Zhao, Z., Tian, J., Sang, Y., Cabot, A., Liu, H., 2015. Structure, synthesis, and applications of TiO_2 nanobelts. Adv. Mater. 27, 2557–2582.
Jing, L., Zhou, W., Tian, G., Fu, H., 2013. Surface tuning for oxide-based nanomaterials as efficient photocatalysts. Chem. Soc. Rev. 42, 9509–9549.
He, W., Kim, H.K., Wamer, W.G., Melka, D., Callahan, J.H., Yin, J. J., 2013. Photogenerated charge carriers and reactive oxygen species in ZnO/Au hybrid nanostructures with enhanced photocatalytic and antibacterial activity. J. Am. Chem. Soc. 136, 750–757.
Wang, Y., Shi, R., Lin, J., Zhu, Y., 2011. Enhancement of photocurrent and photocatalytic activity of ZnO hybridized with graphite-like C 3 N 4. Energy Environ. Sci. 4, 2922–2929.
Li, Peng, Wei, Zhe, Wu, Tong, Peng, Qing, Li, Yadong, 2011. Au−ZnO Hybrid Nanopyramids and Their Photocatalytic Properties. J. Am. Chem. Soc. 133 (15), 5660–5663. https://doi.org/10.1021/ja111102u.
Ansari, S.A., Khan, M.M., Ansari, M.O., Lee, J., Cho, M.H., 2013. Biogenic synthesis, photocatalytic and photoelectrochemical performance of Ag-ZnO nanocomposite. J. Phys. Chem. C. 117, 27023–27030.
Ullah, R., Dutta, J., 2008. Photocatalytic degradation of organic dyes with manganese-doped ZnO nanoparticles. J. Hazard. Mater. 156, 194–200.
Han, Z., Ren, L., Cui, Z., Chen, C., Pan, H., Chen, J., 2012. Ag/ZnO flower heterostructures as a visible-light driven photocatalyst via surface plasmon resonance. Appl. Catal. B 126, 298–305.
Jiang, Y., Sun, Y., Liu, H., Zhu, F., Yin, H., 2008. Solar photocatalytic decolorization of CI Basic Blue 41 in an aqueous suspension of TiO $_2$-ZnO. Dyes Pigm. 78, 77–83.
Shinde, S.S., Bhosale, C.H., Rajpure, K.Y., 2012. Photocatalytic degradation of toluene using sprayed N-doped ZnO thin films in aqueous suspension. J. Photochem. Photobiol., B 113, 70–77.
Qiu, R., Zhang, D., Mo, Y., Song, L., Brewer, E., Huang, X., Xiong, Y., 2008. Photocatalytic activity of polymer-modified ZnO under visible light irradiation. J. Hazard. Mater. 156, 80–85.
Zhang, Z., Yu, Y., Wang, P., 2012. Hierarchical top-porous/bottom-tubular TiO_2 nanostructures decorated with Pd nanoparticles for efficient photoelectrocatalytic decomposition of synergistic pollutants. ACS Appl. Mater. Interfaces 4, 990–996.
Duan, L., Lin, B., Zhang, W., Zhong, S., Fu, Z., 2006. Enhancement of ultraviolet emissions from ZnO films by Ag doping. Appl. Phys. Lett. 88, 232110.
Xie, W., Li, Y., Sun, W., Huang, J., Xie, H., Zhao, X., 2010. Surface modification of ZnO with Ag improves its photocatalytic efficiency and photostability. J. Photochem. Photobiol., A 216, 149–155.
Pathania, D., Kumari, M., Gupta, V.K., 2015. Fabrication of ZnS–cellulose nanocomposite for drug delivery, antibacterial and photocatalytic activity. Mater. Des. 87, 1056–1064.

Pathania, D., Sharma, R., Kalia, S., 2012. Graft copolymerization of acrylic acid onto gelatinized patato starch for removal of metal ions and organic dyes from aqueous system. Adv. Mat. Lett. 3, 259–264.

Yang, J., van Lith, R., Baler, K., Hoshi, R.A., Ameer, G.A., 2014. A thermoresponsive biodegradable polymer with intrinsic antioxidant properties. Biomacromolecules 15, 3942–3952.

Wong, C.M., Zhou, Y., Ng, R.W., Kung, H.F., Jin, D.Y., 2002. Cooperation of yeast peroxiredoxins Tsa1p and Tsa2p in the cellular defense against oxidative and nitrosative stress. J. Biol. Chem. 277, 5385–5394.

Brazel, C.S., Peppas, N.A., 1999. Mechanisms of solute and drug transport in relaxing, swellable, hydrophilic glassy polymers. Polymer 40, 3383–3398.

Pathania, D., Gupta, D., Kothiyal, N.C., Eldesoky, G.E., Naushad, M., 2016. Preparation of a novel chitosan-g-poly (acrylamide)/Zn nanocomposite hydrogel and its applications for controlled drug delivery of ofloxacin. Int. J. Biol. Macromol. 84, 340–348.

Brannon-Peppas, L., Peppas, N.A., 1989. Solute and penetrant diffusion in swellable polymers. IX. The mechanisms of drug release from pH-sensitive swelling-controlled systems. J. Control. Release 8, 267–274.

Khare, A.R., Peppas, N.A., 1993. Release behavior of bioactive agents from pH-sensitive hydrogels. J. Biomater. Sci. Polym. Ed. 4, 275–289.

Alfrey, T., Gurnee, E.F., Lloyd, W.G., 1966. Diffusion in glassy polymers. J. Polym. Sci.: Polym. Symposia 12, 249–261.

Ritger, P.L., Peppas, N.A., 1987a. A simple equation for description of solute release I. Fickian and non-Fickian release from non-swellable devices in the form of slabs, spheres, cylinders or discs. J. Controlled Release 5, 23–36.

Ritger, P.L., Peppas, N.A., 1987b. A simple equation for description of solute release II. Fickian and anomalous release from swellable devices. J. Controlled Release 5, 37–42.

Lin, C.C., Metters, A.T., 2006. Hydrogels in controlled release formulations: network design and mathematical modelling. Adv. Drug Deliv. Rev. 58, 1379–1408.

Kansiz, M., Heraud, P., Wood, B., Burden, F., Beardall, J., McNaughton, D., 1999. Fourier transform infrared microspectroscopy and chemometrics as a tool for the discrimination of cyanobacterial strains. Phytochemistry 52, 407–417.

Liu, X., Li, W., Chen, N., Xing, X., Dong, C., Wang, Y., 2015. Ag-ZnO heterostructure nanoparticles with plasmon-enhanced catalytic degradation for Congo red under visible light. RSC Adv. 5, 34456–34465.

Singh, B., Sharma, V., 2017. Crosslinking of poly (vinylpyrrolidone)/acrylic acid with tragacanth gum for hydrogels formation for use in drug delivery applications. Carbohydr. Polym. 157, 185–195.

Prashar, D., Kaith, B.S., Kalia, S., Sharma, S., 2012. Synthesis, characterization and evaluation of electrical stimulus sensitive behavior of Gt-cl-poly (AA) superabsorbent hydrogel. Int. J. Pharm. Pharm. Sci. 4, 419–423.

Prakash, P., Gnanaprakasam, P., Emmanuel, R., Arokiyaraj, S., Saravanan, M., 2013. Green synthesis of silver nanoparticles from leaf extract of Mimusops elengi, Linn. for enhanced antibacterial activity against multi drug resistant clinical isolates. Colloids Surf., B 108, 255–259. https://doi.org/10.1016/j.colsurfb.2013.03.017.

Lu, Z., Gao, J., He, Q., Wu, J., Liang, D., Yang, H., Chen, R., 2017. Enhanced antibacterial and wound healing activities of microporous chitosan-Ag/ZnO composite dressing. Carbohydr. Polym. 156, 460–469.

Sood, S., Gupta, V.K., Agarwal, S., Dev, K., Pathania, D., 2017. Controlled release of antibiotic amoxicillin drug using carboxymethyl cellulose-cl-poly (lactic acid-co-itaconic acid) hydrogel. Int. J. Biol. Macromol. 101, 612–620.

Trzeciecka, A., Klossowski, S., Bajor, M., Zagozdzon, R., Gaj, P., Muchowicz, A., Malinowska, A., Czerwoniec, A., Barankiewicz, J., Domagala, A., Chlebowska, J., 2016. Dimeric peroxiredoxins are druggable targets in human Burkitt lymphoma. Oncotarget. 7, 1717–1731.

Pathania, D., Gupta, D., Agarwal, S., Asif, M., Gupta, V.K., 2016. Fabrication of chitosan-g-poly (acrylamide)/CuS nanocomposite for controlled drug delivery and antibacterial activity. Mater. Sci. Eng., C 64, 428–435.

Liu, Z., Jiao, Y., Wang, Y., Zhou, C., Zhang, Z., 2008. Polysaccharides-based nanoparticles as drug delivery systems. Adv. Drug Deliv. Rev. 60, 1650–1662.

Pathania, D., Sharma, G., Naushad, M., Kumar, A., 2014. Synthesis and characterization of a new nanocomposite cation exchanger polyacrylamide Ce (IV) silicophosphate: photocatalytic and antimicrobial applications. J. Ind. Eng. Chem. 20, 3596–3603.